Solid silica nanoparticles as carriers of fluorescent squaraine dyes in aqueous media: toward a molecular engineering approach

Gabriele Alberto[a,*], Nadia Barbero[a,*], Carla Divieto[b], Erica Rebba[a], Maria Paola Sassi[b], Guido Viscardi[a], Gianmario Martra[a]

[a] *Department of Chemistry, NIS Interdepartmental and INSTM Reference Centre, University of Torino, Via Pietro Giuria 7, 10125 Torino, Italy*
[b] *Italian National Insititute for Metrological Research INRIM, Strada delle Cacce 91, 10135 Torino, Italy*

E-mail addresses: gabriele.aberto@unito.it, nadia.barbero@unito.it, c.divieto@inrim.it, erica.rebba@unito.it, m.sassi@inrim.it, guido.viscardi@unito.it, gianmario.martra@unito.it
[*] *Corresponding authors*

Keywords: squaraines in water; hybrid dye-silica solid nanoparticles; fluorescence; tissue optical window.

Abstract

Hybrid squaraine-SiO_2 nanoparticles extremely homogeneous in size (50±2 nm), and with photoluminescent emission in the optical tissue window, were prepare by using the reverse microemulsion technique. Three different high quantum-yield squaraine dyes were used and the photophysical behavior of the prepared samples were qualitatively and quantitatively studied, by steady state and time-resolved photoluminescence, in order to establish structure-property relationships useful for the optimization of the preparation method. These squaraine dyes are insoluble in water and suffer a severe decrease of quantum yield if derivatized with polar groups. The role of the hydrophilicity of the dye-APTS adduct in ruling its dispersion in the nascent silica matrix

was confirmed, and the possibility to improve the tuning of the process by properly administration of the adduct with the co-surfactant was demonstrated.

1. Introduction

Organic dyes with absorption in the optical tissue window from 600 to 850 nm (where the self-fluorescence of biological molecules is negligible) have emerged as a promising tool for bioanalytical or biologically related applications and for *in vivo* fluorescence imaging. Polymethine dyes[1], such as cyanines and squaraines, offer numerous advantages such as their easiness in designing new molecules with the desired photochemical properties simply by elongating the central bridge and/or tuning the lateral functional groups[2]. In this manner, dyes with absorption and emission spectra properly located in the optical tissue window are obtained[3]. Cyanines and squaraines have both their own pros and cons, however squaraines, resulting from the dicondensation between squaric acid and electron rich molecules, are typically characterized by a quantum yield and a photostability significantly higher than those found for cyanines[4]. Unfortunately, squaraines are poorly soluble in aqueous media, and the consequent easy formation of non-fluorescent aggregates heavily limited their adoption as fluorescent markers for biological applications. Moreover, the usual strategy used in organic chemistry targeting, i.e. the introduction of a group ionizable in water, such as a sulfonic moiety, is detrimental, because once dissolved in water, such derivatized squaraine dyes show a very low quantum yield with respect to pristine fluorophores dissolved in less polar media[5]. In order to overcome these problems, the incorporation of these hydrophobic dyes in carriers appeared to be a mandatory step for their dispersion in physiological conditions. As far as molecular carriers are concerned, a proposed approach is the encapsulation of the dye inside a permanently interlocked rotaxane molecule, also increasing the resistance to chemical and photochemical degradation[6], or in micelles[7]. Moreover, SQ-based self-assembly in hydrophobic phospholipid bilayers of liposomes were successfully used for *in vivo* imaging[8]. In the domain of inorganic carriers, a possibility is the intercalation of photoactive compounds into hydrotalcite (layered double hydroxides; LDH)[9], or

they can be loaded inside amorphous silica nanoparticles, depending on the specific application. When multifunctional nanoplatforms are pursued, the materials of interest are mesoporous silica nanoparticles, used as such, for instance for photodynamic therapy[10], or wrapped with graphene oxide sheets, to protect the squaric ring from possible nucleophilic attack of molecular components of *in-vitro* and *in-vivo* biological media[11]. When imaging is the intended application, a relevant nanocarrier is constituted by solid non-porous silica nanoparticles (NPs), highly protecting encapsulated dye molecules[12–14]. Hybrid dye doped solid silica NPs can be prepared by hydrolysis and polycondensation of a silicon alkoxide, such as tetraethylorthosilicate (TEOS), and fluorophores derivatized with an alkoxysilane moiety, allowing the encapsulation of dye molecules in the nascent silica matrix. The process can be carried out in homogeneous solution[15], i.e. exploiting the so-called Stöber method, or in reverse microemulsion[16]. In both cases, the condensation reaction among molecular precursors of silica typically occurs by addition of a basic agent, and this can prevent the production of silica NPs hybridized with dyes as penta/hepta-methine cyanines, which do not resist a high pH. Conversely, squaraines do not suffer this limitation, and then appear as relevant organic dyes to be vehiculated in aqueous media by entrapment in silica NPs. Despite the complexity of the synthesis procedure, the microemulsion method can be preferred to the Stöber one, owing to the possibility to obtain particles with a very narrow size distribution, thus simplifying at least one aspect of the complex combination of parameters affecting the behavior of nanomaterials in biological media. Moreover, previous research works devoted to the encapsulation of three methine cyanines[17,18] allowed to highlight that the dispersion of these visible dye molecules throughout the nascent silica matrix is ruled by the relative hydrophilicity of TEOS and the dye-APTS adduct, kinetically competing for the water pool inside reverse micelles[13]. Avoiding aggregation of dyes within the nanocarrier is mandatory to preserve photoemission performances. To the best of our knowledge, no examples of squaraine dyes encapsulated in amorphous silica NPs have been reported so far.

This was the basis of the present work, devoted to the elucidation of molecular aspects and preparation procedures relevant for the production of photoluminescent hybrid squaraines-SiO_2NPs. To this aim, three squaraine dyes with different chemical structures and degree of hydrophilicity (figure 1) were used to synthetize silica NPs by the reverse microemulsion method. Each sample was characterized in terms of size and morphology by electronic transmission microscopy and their photophysical properties were investigated by UV-Vis absorption and steady-state/time-resolved photoemission spectroscopy in order to define structure-property relationships useful for the optimization of the photoemission performances.

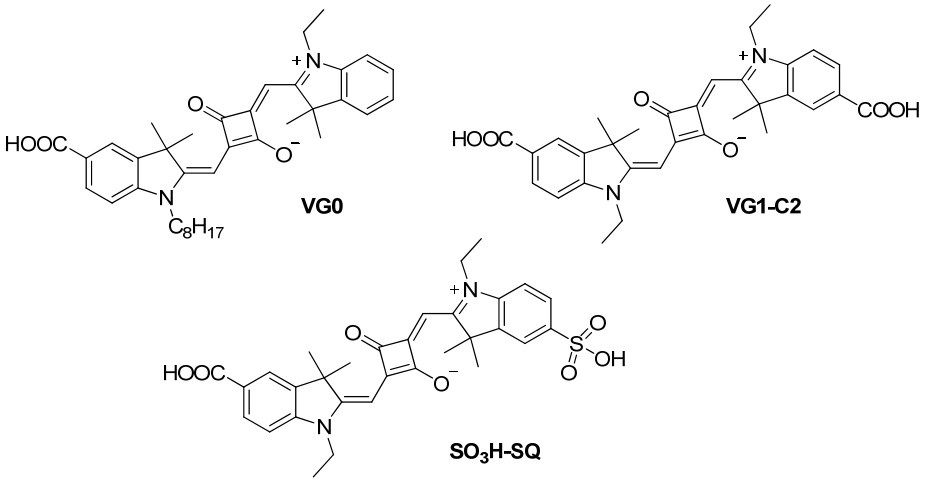

Figure 1. Structures of **VG0**, **VG1-C2** and **SO_3H-SQ**.

2. Experimental details

2.1 Syntheses: chemicals and procedures

All reagents and solvents, of a highly pure grade, were purchased from Sigma Aldrich, Fluka, Merck or Riedel de Haen and were used without any further purification.

2.1.1 Synthesis of squaraines

VG0 and **VG1-C2** were prepared as previously described[2]. For the synthesis of **SO_3H-SQ** a modified procedure as reported in the literature [2,19] was followed. An equimolar mixture (0.84 mmol) of compound **1** and **2** (scheme 1) were introduced into a 20 ml microwave reaction vial with

toluene and butanol (18 ml, 1:1), sealed with a crimp cap and heated in the microwave system (single-mode Biotage Initiator 2.5) at 160°C for 25 min. The green precipitate which is formed is washed with diethyl ether and further purified by a semi-preparative HPLC system (by Schimatzu, equipped with SCL 10Avp, SPD 10Avp, a LC8A pump and a Phenomenex column Synergi Fusion-RP 4 µ, 150x21.20 mm) using an isocratic flow of methanol with formic acid (1%, v/v) to obtain SO_3H-SQ (105 mg, yield = 22%) as a green powder.

^1H NMR (200MHz, D_2O), δ: 8.01-7.72 (m, 6H), 7.15 (s, 1H), 6.91 (s, 1H), 4.42 (m, 2H), 3.79 (m, 2H), 1.47 (s, 12H), 1.14 (s, 6H).

MS (ESI) $[M-H]^-$ 575.60

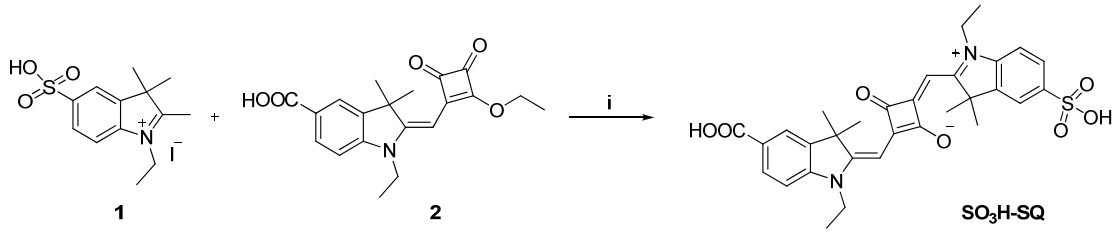

Scheme 1. Synthesis of SO_3H-SQ. Experimental conditions: (i) toluene/butanol (1:1), MW, 25 min, 160°C.

2.1.2 Synthesis of squaraine-silane derivatives

The *N*-Hydroxysuccinimide (NHS) active esters of the two non-symmetrical squaraines VG0 and SO_3H-SQ were synthetized by reacting 0.02 mmol of each fluorophore with NHS (0.08 mmol) and N,N'-Dicyclohexylcarbodiimide (DCC, 0.08mmol) in dimethylformamide (DMF, 2.0 ml) and stirring for 4h at 80°C; in the case of the symmetrical VG1-C2, 0.16 mmol of both NHS and DCC were used due to the presence of two carboxyl groups. Reactions were monitored by mass spectrometry until complete conversion and then the product was separated through dilution in diethyl ether and filtration to obtain products as powders.

Squaraine-silane derivatives were then prepared by adding 3-aminopropyltriethoxysilane (APTS; 46.0 µmol, 10 µL for VG0-NHS and SO_3H-SQ-NHS; 92.0 µmol, 20 µL for VG1-C2-NHS) to

squaraine-NHS solutions in 0.5 ml of anhydrous DMF and stirring the mixture for 24h at room temperature; reactions were monitored by thin layer chromatography until complete disappearance of former NHS esters. The obtained squaraine-silane derivatives (hereafter X-APTS, where X is the squaraine code) were then used without further purification in order to avoid the occurrence of self-polymerization.

Schemes of the syntheses are shown in the Supporting Information (hereafter SI).

2.1.3 Synthesis of squaraine-loaded silica NPs

Hybrid squaraine-silica NPs were prepared by the reverse microemulsion technique already reported in previous works[17,18,20]. Briefly, a water in oil microemulsion was prepared by mixing cyclohexane (75.0 ml), Triton X-100 (18.85 g), *n*-hexanol (18.0 ml) and distilled water (5.4 ml); the mixture was gently stirred for ca. 30 minutes and then 0.05 ml of a 0.01 M squaraine-APTS in DMF was added; after further 15 minutes, TEOS (1.0 ml, 4.5 mmol) and NH_4OH (28-30%, 0.7 ml) were added to start the NPs formation. Reaction was stirred for 16 hours at room temperature and then was stopped by adding 50.0 ml of acetone; particles were extracted from the supernatant by centrifugation (10k rpm, r.t.) and washed twice in ethanol and several times in distilled water by resuspension and centrifugation cycles until complete removal of the surfactant. Finally, squaraine-loaded silica NPs (hereafter X-NPs, where X is the squaraine code) were stored as suspensions in distilled water at room temperature in the dark until needed.

In order to attain possible optimization of the preparation technique, in two cases the hybrid NPs preparation protocol was changed (*vide infra*) and the resulting materials were labeled as X-NPs-B.

For solvatochromic experiments, NPs stored as water suspensions were first centrifuged at 10k rpm for 20 minutes and then resuspended using acetone. Then, NPs were washed twice by centrifugation/resuspension cycles in order to completely remove water and, finally, the concentration of the final suspensions was adjusted to 1 $mg \cdot ml^{-1}$.

2.2 Methods

2.2.1 Characterization of dyes

Thin-layer chromatography was performed on silica gel 60 F254 plates. ESI-MS spectra were recorded using a LCQ Thermo Advantage Max spectrometer, with electrospray interface and ion trap as mass analyzer. The flow injection effluent was delivered into the ion source using nitrogen as sheath and auxiliary gas. ^{1}H NMR (200 MHz) spectra were recorded on a Bruker Avance 200 NMR.

2.2.2 UV-Vis absorption spectroscopy

UV-VIS electronic absorption spectra of the squaraine in solution and of the supernatants derived from nanoparticle extraction from the microemulsion mixture were measured by a Cary 300 Bio spectrophotometer (Varian, Santa Clara, CA, USA), using quartz cuvettes (1 cm pathway length).

For the determination of absorption coefficients, every dye was weighed, (7.0-10.0 mg), and diluted to 10.0 ml in a flask using DMSO. From this solution, 0.25 ml were taken and diluted to 25.0 ml with the proper solvent (mother solution). Three dilutions were prepared by diluting 1.0, 2.5 and 5.0 ml of this solution to 25.0 ml. Those solutions were analyzed by UV-Vis spectroscopy. Absorbance at the λ_{max} for every diluted solution was plotted vs. dye concentration and a linear fitting was performed. The slope of the plot is the molar absorption coefficient (ε). The determination was made, in duplicate, by preparing two separate concentrated dye mother solutions in DMSO. The logε obtained from the two separate data sets was compared: if their difference was less or equal to 0.02 respect to their average, the data were considered acceptable and the average of the two values was taken as the official value. Otherwise, a further concentrated dye mother solution in DMSO was prepared, the whole procedure was repeated and the logε data were compared.

2.2.3 UV-Vis photoemission spectroscopy

Photoluminescence and excitation spectra in steady state mode were acquired using a Horiba Jobin Yvon Fluorolog 3 TCSPC fluorimeter equipped with a 450-W Xenon lamp and a Hamamatsu R928 photomultiplier.

The absolute quantum yield of each dye in solution was determined combining Quanta-φ with Fluorolog 3. The reported values are the average of three measurements using three different dye solutions.

Fluorescence lifetimes were measured by the time correlated single photon counting method (Horiba Jobin Yvon) using a 560 nm Horiba Jobin Yvon NanoLED as excitation source and an impulse repetition frequency of 1 MHz positioned at 90° with respect to a TBX-04 detector. Lifetimes were calculated using DAS6 decay analysis software.

2.2.4. High resolution transmission electron microscopy (HRTEM)

Size and morphology of NPs were analyzed with a 3010 Jeol microscope operating at 300 kV. A droplet of each nanoparticle water suspension (1.0 mg ml^{-1}) was spread on a copper grid coated with a carbon film and then water was allowed to slowly evaporate in order to limit particle agglomeration. Size distribution was evaluated by measuring at least 300 nanoparticles and the mean diameters were calculated as $d_m = \Sigma d_i n_i / \Sigma n_i$ (n_i= number of particles of diameter d_i); results were reported as $d_m \pm$ stdv.

3. Results and discussion

3.1 Synthesis of squaraines and squaraine-silane derivatives

VG0 and **VG1-C2** squaraines were prepared via a microwave condensation reaction based on a previously reported procedure[2] while **SO_3H-SQ** was synthesized by a microwave-assisted condensation of 5-sulfo-indolenine salt **1**[19] and carboxyemisquarate **2**[2] (see Scheme 1).

Squaraine-silane derivatives were prepared via a previously reported method [12] through the NHS ester modification of the squaraine carboxylic group and subsequent reaction with APTS (see Scheme S2 in the SI for **SO_3H-SQ** modification).

3.2 Photophysical properties of squaraines in solution

The photophysical behaviour of each squaraine dye in solution was investigated together with the determination of the correspondent molar decadic absorption coefficient and absolute quantum yield by means of absorption and both steady-state and time-resolved photoemission spectroscopies (see Table 1).

The UV-Vis absorption spectra (see Figure 2) of the squaraine dyes show absorption maxima between 630 nm and 646 nm with high molar extinction coefficients (logε around 5.40 in organic solvents and 4.51 in water). The main absorption peak is associated to the $\pi \rightarrow \pi^*$ HOMO–LUMO transitions, mainly localized on the squarainic core[21,22], while the shoulder at higher energy is due to the HOMO-LUMO+1 transition. When excited within the absorption band at room temperature, the three types of squaraines emit a luminescence spectrum almost specular to the absorption one, with maxima ranging from 639 to 656 nm, thus with small Stokes shifts as expected for squaraine dyes[23].

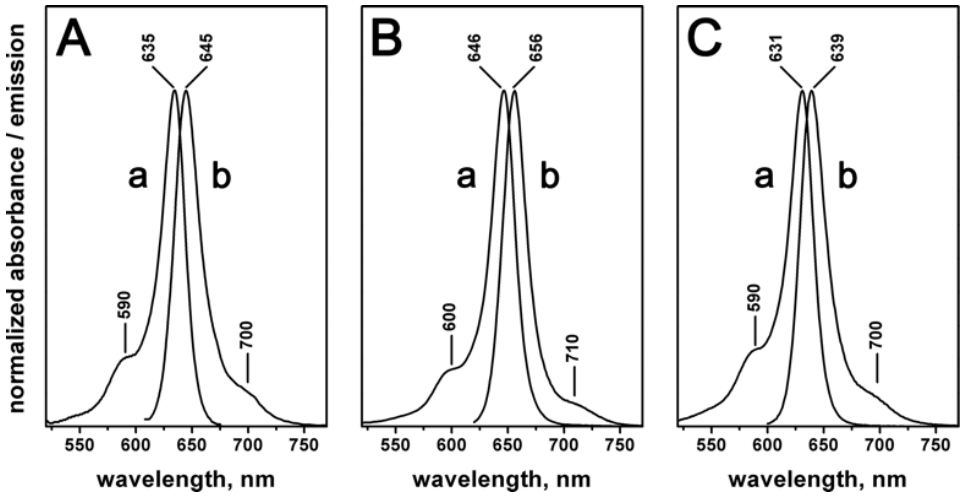

Figure 2. Absorption (a) and emission spectra (λ_{ex}= 590 nm) (b) of **VG0** in methanol (panel A), **VG1-C2** in acetone (panel B) and **SO_3H-SQ** in water (panel C).

Fluorescence lifetime and quantum yield of VG0 in methanol and VG2-C1 in acetone are in the ranges typical for squaraines in organic media [24]. Also the much lower τ and Φ of SO_3H-SQ is in agreement with the expected photoemission behaviour in water due to a non-radiative loss of the excitation energy during vibrational relaxation of water molecules.[25,26]

Table 1. Main optical characteristics of **VG0** in methanol, **VG1-C2** in acetone and **SO_3H-SQ** in water.

	λ_{abs} (nm)	logε	λ_{em} (nm)	τ (ns)	φ
VG0†	635	5.39	645	0.28 (100%)	0.15
VG1-C2*	646	5.40	656	0.99 (100%)	0.27
SO_3H-SQ	631	4.51	639	0.11 (100%)	0.023

† in methanol, * in acetone, in water

3.3 Shape, size and dye-content of squaraine loaded silica NPs

Representative TEM micrographs of the three squaraine-NPs samples are shown in figure 3, where the highly regular spherical shape (upper panels) and quite homogeneous size of NPs around a mean diameter of 50 nm (lower panels) can be appreciated. Hence, on the basis of the TEOS-to-SiO_2 conversion yield, the density of NPs (ca. 2.2 $g \cdot cm^{-3}$)[18] and the calculated average nanoparticle volume, the total number of NPs obtained by each preparation was estimated.

As a second step, for each sample the total amount of squaraine molecules associated to NPs was calculated as the difference between their initial amount and that remained in the reaction media after the accomplishment of the formation of NPs, as determined spectrophotometrically after the separation of NPs by centrifugation. This was possible because no squaraine degradation products were detected in the UV-Vis spectra of the post-reaction liquid medium. Thus, the average number of dye molecules per nanoparticle was calculated (Table 2). Apparently, the VG0-APTS adduct was unable to participate to the formation of NPs, whereas this was the case for ca. 45 % and 65% of

VG1-C2-APTS and SO_3H-SQ-APTS species present in the relevant reaction media, resulting in ca. 50 and 70 dye molecules-per-NP, respectively.

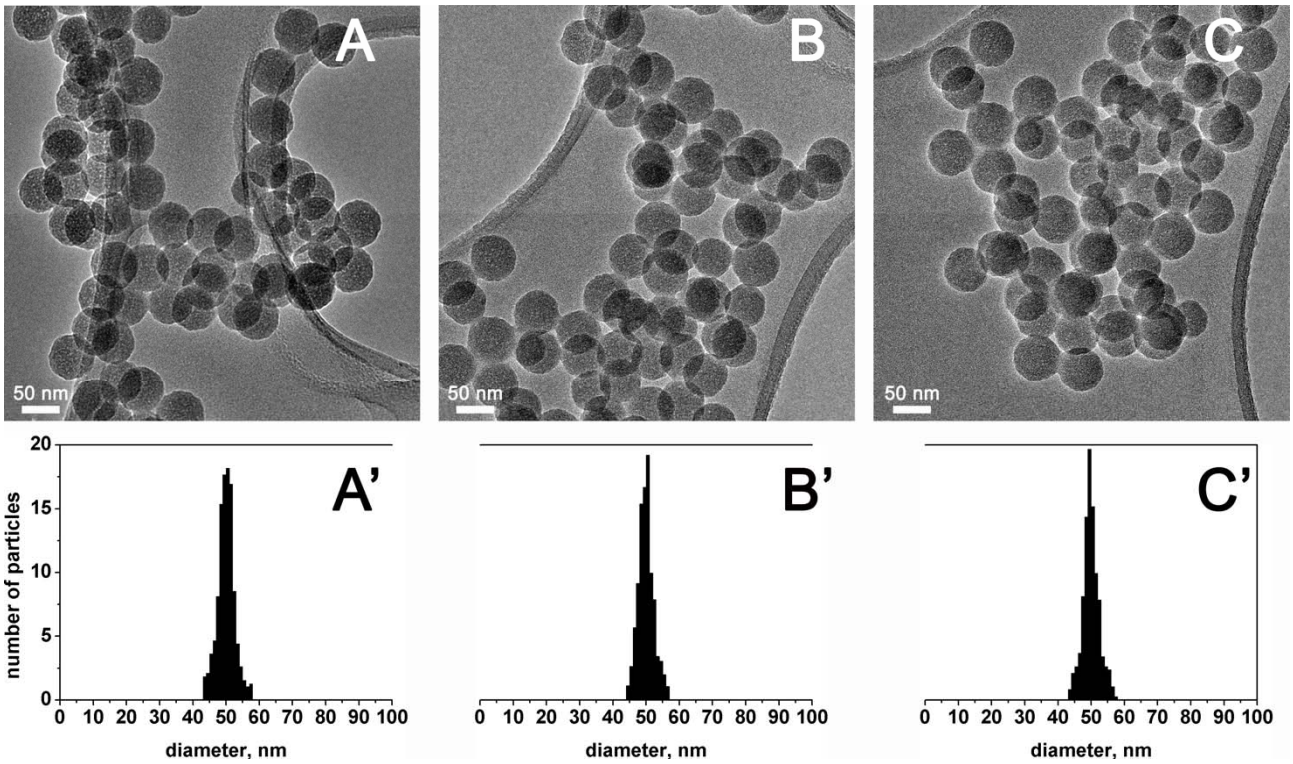

Figure 3. Representative TEM images of VG0-NPs (A), VG1-C2-NPs (B) and SO_3H-SQ-NPs (C) and correspondent size distribution histograms. Original magnification of images: 500000×. Scale bar: 50 nm

Table 2. Yields of entrapment of squaraine-APTS molecules in silica NPs

	Yield of Squaraine-APTS molecules entrapment (%)	**Squaraine-APTS molecules per NP (n°)**
VG0-NPs	0	0
VG1-C2-NPs	46	47
SO_3H-SQ-NPs	66	68
VG1-C2-NPs-B	41	42
SO_3H-SQ-NPs-B	63	65

The lack of encapsulation of VG0-APTS in the silica matrix should be rationalized in terms of a so poor hydrophilicity of this squaraine derivative to prevent its transfer into the water pool in the core of reverse micelles, and thus this squaraine derivative will be no longer considered. Conversely, the presence of two triethoxysilane moieties in VG1-C2-APTS counterbalance enough the hydrophobicity of the squaraine motif to allow this derivative to reach the water pools and participate to hydrolysis and condensation with TEOS during the formation of NPs. As expected, a stronger effect resulted from the presence of the sulphonic group in SO_3H-SQ-APTS, which was involved in the formation of NPs in a larger extent. However, the rate of transfer into the micelles of neither VG1-C2-APTS nor SO_3H-SQ-APTS was high enough to allow all the dye derivative to participate to the reaction before the accomplishment of the formation of the NPs.

3.4 Photoemission properties and location of the entrapped squaraines

In order to evaluate any possible modification of the photophysical behaviour of the entrapped fluorophores, steady state photoemission and excitation spectra of hybrid VG1-C2-NPs and SO_3H-SQ-NPs were recorded in suspension and compared to the data obtained for the correspondent dye derivatives in solution (figure 4). Data obtained for VG1-C2 and VG1-C2-APTS were similar, indicating that the derivatization did not modify significantly the photophysical behaviour of the dye. SO_3H-SQ was only soluble in water, and this prevented a comparison with SO_3H-SQ-APTS in the same medium, because of the sensitivity of the derivative to hydrolysis. Thus, the pristine VG1-C2 and SO_3H-SQ were considered for the comparisons with their derivative associated to NPs.

For both types of hybrid NPs, excitation instead of absorption in transmission was recorded because the lower sensitivity of the latter did not allow to record spectra with an acceptable signal-to-noise ratio at suspension concentrations low enough to avoid light scattering.

In figure 4 panel A, excitation and photoemission spectra of VG1-C2 in solution and VG1-C2-NPs in suspension are reported; acetone was used as solution and suspension medium due to the low solubility of VG1-C2 in water. It can be clearly observed that both excitation and emission signals of

the NPs are identical to the correspondent ones of the fluorophore in solution suggesting that no modifications of the energies and probabilities of the electronic transitions occurred due to the association with the inorganic matrix. On the contrary, in the case of SO_3H-SQ (figure 4, panel B),

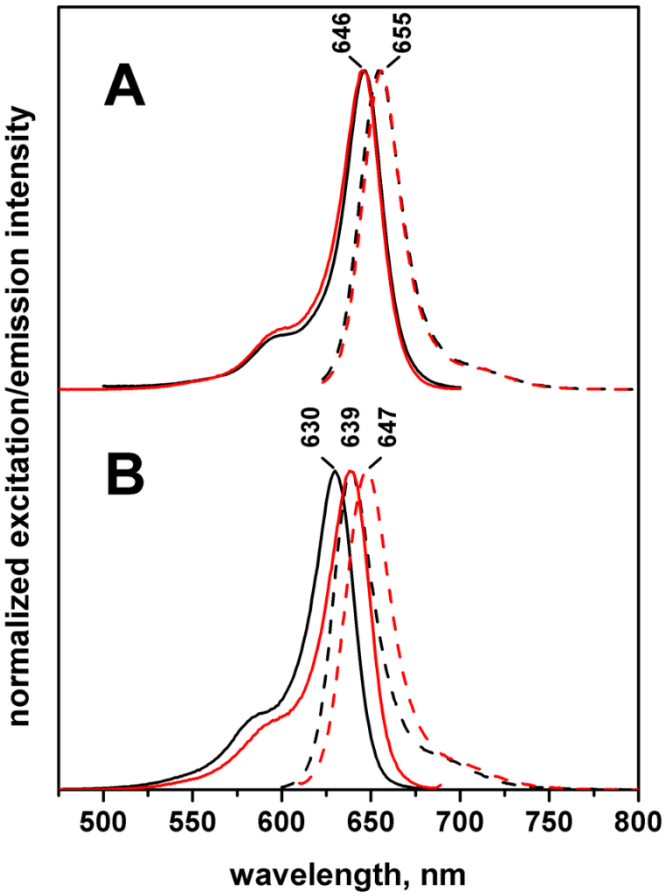

Figure 4. Panel A: excitation (solid curves, λ_{em} = 655 nm) and photoemission (dashed curves, λ_{exc} = 590 nm) spectra of VG1-C2 in acetone solution (black curve, $5.0 \cdot 10^{-6}$ M) and VG1-C2-NPs in acetone suspension (red curve, $3.0 \cdot 10^{-8}$ mg·ml^{-1}); Panel B: excitation (solid curves, λ_{em} = 640 nm) and photoemission (dashed curves, λ_{exc} = 590 nm) spectra of SO_3H-SQ in water solution (black curve, $5.0 \cdot 10^{-6}$ M) and SO_3H-SQ-NPs in water suspension (red curve, $3.0 \cdot 10^{-8}$ mg·ml^{-1}). All spectra were normalized with respect to the maximum for the sake of clarity.

where the hydrophilicity of the dye allowed to use water as medium for both the molecule in solution and the hybrid NP suspension, the association of dye derivatives with silica produced a decrease of the energies of absorption and fluorescence transitions as indicated by the 9 nm red shift of both signals. The coincidence of the shape of the spectra profiles exhibited by both dye/hybrid NPs pairs allowed to exclude the occurrence of intra-particle autoabsorption effects. Hence, as the framework

of amorphous silica is apolar[27] the red-shift observed for SO_3H-SQ-NPs should be reasonably assigned to a solvatochromic effect due to the decrease of the polarity of the environment experienced by entrapped squaraine derivatives with respect to the ones in water solution. The solvathocromic behavior of the SO_3H-SQ in solution were reported in figure S1 in the SI for the sake of comparison. Time-resolved photoemission measurements were also carried out, and the results are listed in table 3, compared with relevant cases of squaraine derivatives in solution. The targeted suspension medium for hybrid NPs is water, but also acetone was considered because of its lower polarity, thus useful to reveal possible solvatochromic effects due to dye molecules not entrapped in the bulk of NPs. For all suspensions of hybrid NPs, bi-functional equations were necessary to fit the decay curves, indicating that for both VG1-C2-APTS and SO_3H-SQ-APTS derivatives two different scenarios of interaction with the silica host are present. For VG1-C2-APTS, independently on the suspension medium, one fluorescence lifetime (τ^0_F) is slightly longer than what found for the molecular form in acetone solution, whereas the other (τ^1_F) appears increased of ca. 2.5 times with respect to that comparative form. In the case of SO_3H-SQ-APTS, the association with the silica matrix resulted in two lifetimes both significantly longer than for the molecular form in water solution, with an increase of ca. 7-10 and ca. 20 times, for τ^0_F and τ^1_F, respectively. For both types of hybrid dye-SiO_2 NPs, the relative population of fluorescent molecules showing the longer lifetime is the more abundant by far.

For hybrid dye-NPs, the increase of fluorescence lifetime is the result of the decrease in rotational degrees of freedom, and in possible detrimental effects due to the interaction with highly polar media, such as water. Thus, data obtained for SO_3H-SQ-NPs indicate that SO_3H-SQ derivatives should be not simply anchored on the surface of NPs. Because of the similarity of τ^1_F values, significantly longer than the fluorescence lifetime of VG1-C2-APTS in acetone solution, the same should occur at least for the most abundant fraction of fluorescent dyes in VG1-C2-NPs. Conversely, the other fraction should experience an interaction with its environment with more limited differences with respect of acetone as solvent.

Noticeably, the time resolved photoemission behavior of both VG1-C2-NPs and SO_3H-SQ-NPs appeared sensitive to the suspension medium, with a slight increase of both τ^0_F and τ^1_F and, more significantly, with the transfer of ca. a 10% of fluorescent molecules between the relative abundances of dyes showing different fluorescence lifetime.

Table 3. Emission decay times (λ_{exc} = 560 nm) of: VG1-C2 in acetone solution ($5 \cdot 10^{-7}$M); VG1-C2-NPs and VG1-C2-NPs-B in acetone and water suspension (0.1 mg·ml^{-1}); SO_3H-SQ in water solution ($1 \cdot 10^{-6}$ M); SO_3H-SQ-NPs and SO_3H-SQ-NPs-B in water and acetone suspension (0.1 mg·ml^{-1})

	Medium	τ^0_F (ns)	% τ^0_F (ns)	τ^1_F (ns)	% τ^1_F (ns)	χ^2
VG1-C2	acetone	0.99	100	---	---	1.01
VG1-C2-NPs	acetone	1.19	21	2.42	79	1.12
	water	1.06	31	2.37	69	1.04
SO_3H-SQ-NPs	acetone	1.10	15	2.38	85	1.08
	water	0.80	21	2.31	79	1.02
SO_3H-SQ	water	0.11	100	---	---	1.03
VG1-C2-NPs-B	acetone	1.35	25	2.44	75	1.04
	water	1.02	43	2.19	57	1.13
SO_3H-SQ-NPs-B	acetone	1.21	35	2.62	65	1.07
	water	0.99	46	2.38	54	1.02

For both VG1-C2-NPs and SO_3H-SQ-NPs, fluorescent dyes showing the longer lifetime are candidate to be depicted as well entrapped in the silica matrix; however, their sensitivity to the suspension medium, and in particular their change in relative abundance, pose a problem.

In this respect, it is useful to remind that silica NPs prepared by the microemulsion or Stöber methods are characterized by the presence of domains, extended from the surface towards the interior, of non-completely condensed silica, resulting in a mass fractal structure sensitive to changes in the external environment [28,29]. Moreover, H/D isotopic exchange indicated that such domains can be infiltrated by water molecules[21]. Therefore, although the sensitivity of the measurement technique

did not allow to distinguish more than two relative abundances of fluorescent dyes for each type of hybrid NPs, the obtained data could be explained by assuming the presence of three ensembles of fluorescent dyes in the NPs (scheme 2):

i) a most abundant fraction, characterized by the longer fluorescent lifetime, τ^1_F (ca.70% and 80% for VG1-C2-NPs and SO_3H-SQ-NPs, respectively), well constrained by the silica matrix, likely in its fully condensed part, insensitive to changes in suspension medium

ii) a fraction of ca. 20% for VG1-C2-NPs and 15% for SO_3H-SQ-NP, showing the shorter fluorescent lifetimeτ^0_F, located at/near the nanoparticle surface and less constrained by the silica matrix independently on the type of suspension medium

iii) a fraction, ca. 10% and 6% for VG1-C2-NPs and SO_3H-SQ-NPs, respectively, located in not fully condensed parts of silica matrix more sensitive to the nature of the suspension medium, where fluorescent dyes are less constrained when these parts are infiltrated by water.

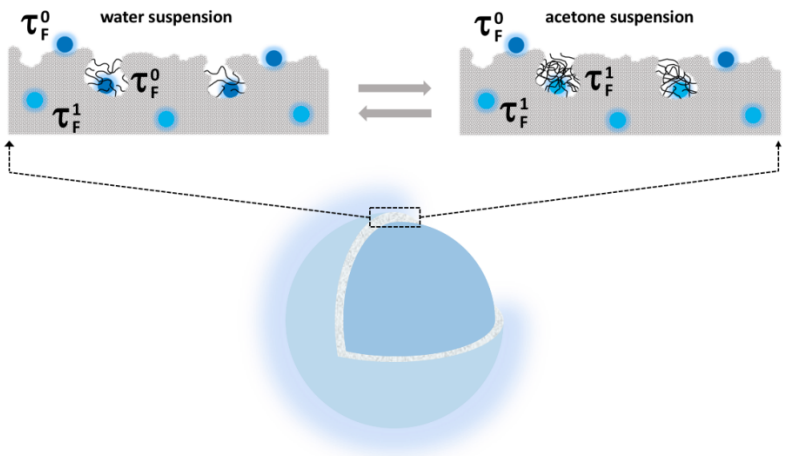

Scheme 2. Distribution of dye molecules in the NPs explaining the different sensitivity to the suspension medium

3.5 Dyes in solution vs hybrid NPs: comparison of fluorescence intensity

Because of the direct proportionality between fluorescence lifetime and quantum yield[30], the measured increase of fluorescence lifetime for all dye fractions in SO_3H-SQ-NPs and the most

abundant one for VG1-C2-NPs appears the basis for expecting an increase in fluorescence intensity of hybrid NPs suspensions with respect to the squaraine derivatives in solutions, for equivalent dye molar concentrations. Hence, the following experimental procedure was used for VG1-C2 and SO_3H-SQ-based systems, differing only for the suspension medium, as described in the previous section. On the basis of the calculated number of squaraine per nanoparticle (table 2), a series of suspensions at known dye concentration was prepared for both VG1-C2-NPs and SO_3H-SQ-NPs, as well as a series of solutions of VG1-C2 and SO_3H-SQ in the same concentration range. The photoemission spectra were recorded, strictly using the same excitation conditions, and the integrated intensities of photoemission spectra were plotted with respect to the correspondent concentration values (figure 5). A straight linear dependence was obtained, clearly indicating that the measurements were affected by neither light scattering nor inter-particle auto-absorption effects.

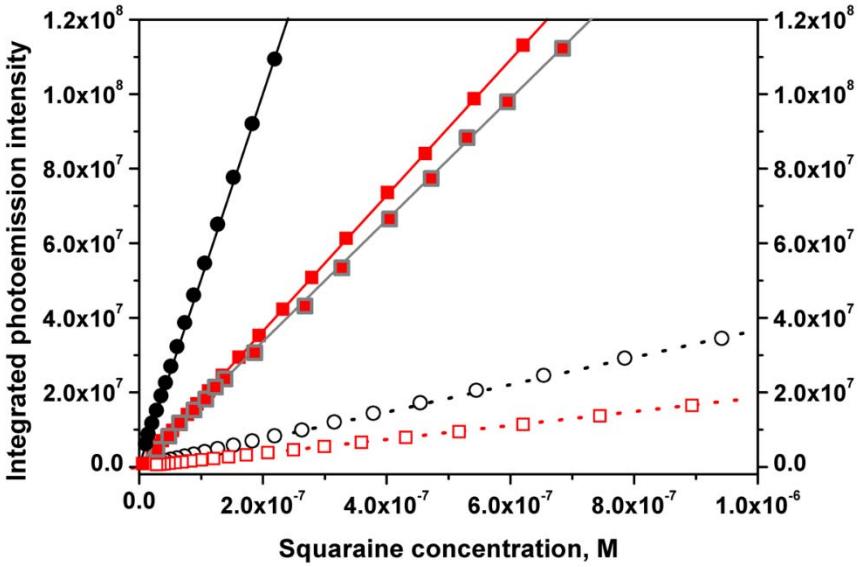

Figure 5. Comparison of the integrated intensities of photoemission spectra (λ_{exc} =590 nm) of VG1-C2 in acetone solution (black solid dots), VG1-C2-NPs in acetone and water suspension (red solid squares and grey bordered red squares, respectively), SO_3H-SQ in water solution (black empty dots) and SO_3H-SQ-NPs in water suspension (red empty squares)

In agreement with the absolute quantum yields (table 1), solutions of the two squaraines produces significantly different fluorescence outputs, with VG1-C2 (black solid dots) showing integrated

intensities of photoemission spectra ca. 13 times higher than SO_3H-SQ (black empty dots). Conversely, data obtained for the hybrid NPs were not in agreement with expectations: the integrated intensities of photoemission spectra of VG1-C2-NPs in both acetone (red solid squares) and water (grey borded red squares) suspensions are ca. 35% and 30%, respectively, of what obtained for VG1-C2 solutions (black solid dots), and the relative decrease is limited to ca. 50% when comparing the SO_3H-SQ-NPs/SO_3H-SQ pair (red empty squares and black empty dots, respectively).

Such lower than expected fluorescence intensity should be due to a decrease of the decadic absorption coefficient of squaraines and/or a quenching of a part of them when linked to/entrapped in the silica matrix. Non-light-scattering suspensions of hybrid NPs were too diluted to allow the recording of absorbance spectra, and then no insights were obtained for the first possibility.

Focusing on fluorescence quenching, if occurred it might be of the concentration type, resulting from the formation of aggregates of squaraine derivatives when involved in the growth of NPs. In particular, SO_3H-SQ-APTS, highly hydrophilic and then easily transferred from the oil phase to the inner water pool of reverse micelles, could have formed aggregates in the first steps of the reaction, whereas the contrary might have occurred for VG1-C2-APTS, definitely less hydrophilic and then involved in the reaction when the nanoparticle formation was almost accomplished.

Based on these hypotheses, two additional samples were prepared by modifying the synthesis procedure with an opposite target, depending on the squaraine derivative considered. Thus, to dilute in time the entering of SO_3H-SQ-APTS in the micelles, the adduct was dosed in the reaction medium in small aliquots at regular time intervals (0.01 ml every 10 min) during the first hour of the NPs synthesis. Conversely, VG1-C2-APTS was added to the microemulsion as solution in *n*-hexanol, i.e. the co-surfactant of micelles, in order to facilitate its partition at the boundary between the oil and water phases. In this way, the shortening of the diffusion path should allow this squaraine derivative to be involved not only in late steps of the formation of NPs. These two samples were labeled as SO_3H-SQ-NPs-B and VG1-C2-NPs-B.

As for the previous cases, the amount of dyes effectively associated with NPs was calculated, and values very close to the ones already found for the previous corresponding hybrid NPs were obtained (table 2). The same occurred for steady-state and time resolved photoemission data (Figure S2 in the SI and table 3, respectively). Conversely, the integrated intensity of the photoemission spectra of dye equimolar SO_3H-SQ solutions/hybrid NPs suspensions in water appears almost coincident, while the values obtained for VG1-C2-NPs-B in acetone and water suspensions are ca. 90% and 70%, respectively of those measured with VG1-C2 in acetone solutions (figure 6). Thus, the second set of hybrid NPs shows a definitely better performance as photoemitters with respect to the first one (see figure 5).

Apparently, the strategies adopted to affect the distribution of squaraine derivatives on/in the silica NPs were successful, at least partly. In fact, if all dye molecules in hybrid NPs were fluorescent, based on the measured increase in photoemission lifetime, the fluorescence intensity of their suspensions should exceed that of equimolar dye solutions by far. A specific investigation in this respect will be the object of a future investigation.

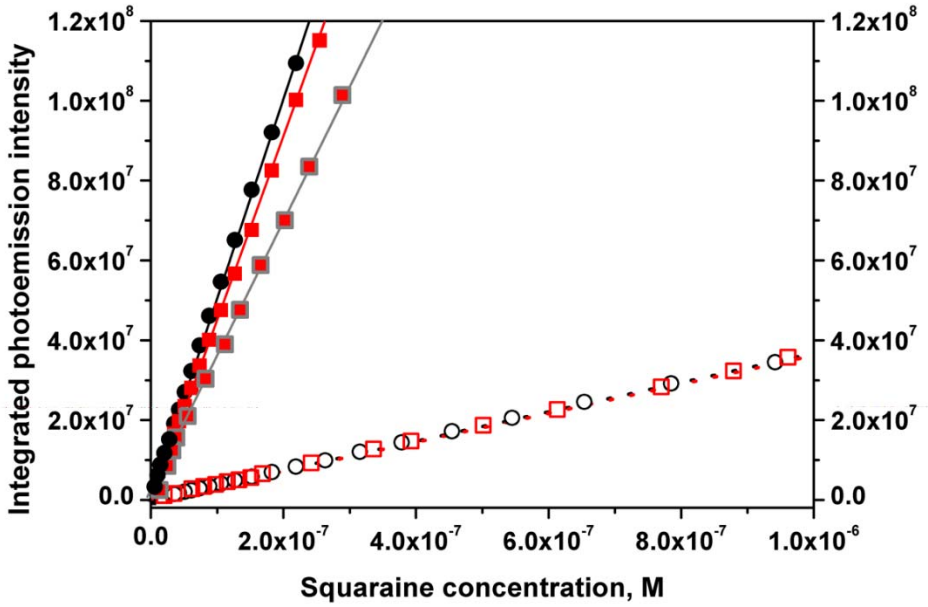

Figure 6. Comparison of the integrated photoemission intensities (λ_{exc} =590 nm) of VG1-C2 in acetone solution (black solid dots), VG1-C2-NPs-B in acetone and water suspension (red solid

squares and grey bordered red squares, respectively), SO_3H-SQ in water solution (black empty dots) and SO_3H-SQ-NPs-B in water suspension (red empty squares).

4. Conclusion

The preparation of hybrid squaraines-silica nanoparticles has been achieved successfully by the reverse microemulsion method. They show, in aqueous suspension, a photoluminescence emission intensity, per dye molecule, equivalent to parent water unsoluble squaraine molecules, when in organic solution, Such achievement stems from the adopted molecular engineering approach, based on the hypothesis that the relative hydrophylicity of dye-3-aminopropyltriethoxysilane (APTS) adducts and tetraethylorthosilicate (TEOS) is a key parameter ruling the distribution of fluorophores within the nascent silica matrix. Such hypothesis, developed in previous studies on the preparation of hybrid cyanine- SiO_2 nanoparticles[21], and recently assumed also by other researchers[31], has been here confirmed also for squaraines. In addition, the possibility to improve the tuning of the process by administering the squaraine-APTS adduct with the co-surfactant has been demonstrated. This is the first report, at the best of our knowledge, on molecular factors ruling the dispersion of squaraines in solid silica nanoparticles, but the number of dye molecules per nanoparticles and likely their photoluminescent fraction are significantly lower with respect what obtained with cyanine dyes [19, 21]. Thus, the future steps of this research will be aimed to overcome this gap, targeting brighter hybrid squaraine-SiO_2 nanoparticles.

Acknowledgments

This work was supported by the Fondazione Cassa di Risparmio di Torino, Italy (STemMRef project, cod. ID 48853).

References

[1] S. Luo, E. Zhang, Y. Su, T. Cheng, C. Shi, A review of NIR dyes in cancer targeting and

imaging, Biomaterials. 32 (2011) 7127–7138. doi:10.1016/j.biomaterials.2011.06.024.

[2] N. Barbero, C. Magistris, J. Park, D. Saccone, P. Quagliotto, R. Buscaino, C. Medana, C. Barolo, G. Viscardi, Microwave-assisted synthesis of near-infrared fluorescent indole-based squaraines, Org. Lett. 17 (2015) 3306−3309.

[3] L. Serpe, S. Ellena, N. Barbero, F. Foglietta, F. Prandini, M.P. Gallo, R. Levi, C. Barolo, R. Canaparo, S. Visentin, Squaraines bearing halogenated moieties as anticancer photosensitizers: Synthesis, characterization and biological evaluation, Eur. J. Med. Chem. 113 (2016) 187–197. doi:10.1016/j.ejmech.2016.02.035.

[4] H. Zollinger, Color Chemistry, Second Edi, VCH, Weinheim, 1991.

[5] I.A. Karpenko, A.S. Klymchenko, S. Gioria, R. Kreder, I. Shulov, P. Villa, Y. Me, M. Hibert, D. Bonnet, Squaraine as a bright, stable and environment- sensitive far-red label for receptor-specific cellular imaging, Chem. Commun. 51 (2015) 2960–2963. doi:10.1039/C4CC09113B.

[6] E. Arunkumar, N. Fu, B.D. Smith, Squaraine-Derived Rotaxanes : Highly Stable , Fluorescent Near-IR Dyes, Chem. - A Eur. J. 12 (2006) 4684–4690. doi:10.1002/chem.200501541.

[7] S. Sreejith, J. Joseph, M. Lin, N.V. Menon, P. Borah, Near-Infrared Squaraine Dye Encapsulated Micelles for in Vivo Fluorescence and Photoacoustic Bimodal Imaging, ACS Nano. 9 (2015) 5695–5704. doi:10.1021/acsnano.5b02172.

[8] F. Wu, H. Wang, Nano-Con fi ned Squaraine Dye Assemblies: New Photoacoustic and Near-Infrared Fluorescence Dual-Modular Imaging Probes in Vivo, Bioconjug. Chem. 25 (2014) 2021−2029. doi:10.1021/bc5003983.

[9] E. Conterosito, I. Benesperi, V. Toson, D. Saccone, N. Barbero, L. Palin, C. Barolo, V. Gianotti, High-Throughput Preparation of New Photoactive Nanocomposites, Chem. Sus. Chem. 9 (2016) 1279–1289. doi:10.1002/cssc.201600325.

[10] I. Miletto, A. Fraccarollo, M. Cossi, L. Marchese, N. Barbero, C. Barolo, Mesoporous silica

nanoparticles incorporating squaraine-based photosensitizers: a combined experimental and computational approach, Dalt. Trans. (2018) 15–18. doi:10.1039/c7dt03735j.

[11] S. Sreejith, Y. Zhao, Graphene Oxide Wrapping on Squaraine-Loaded Mesoporous Silica Nanoparticles for Bioimaging, J. Am. Chem. Soc. 134 (2012) 17346−17349. doi:10.1021/ja305352d.

[12] S. Santra, D. Dutta, B.M. Moudgil, Functional dye-doped silica nanoparticles for bioimaging, diagnostics and therapeutics, Food Bioprod. Process. 83 (2005) 136–140. doi:10.1205/fbp.04400.

[13] L. Accomasso, E.C. Rocchietti, S. Raimondo, F. Catalano, G. Alberto, A. Giannitti, V. Minieri, V. Turinetto, L. Orlando, S. Saviozzi, G. Caputo, S. Geuna, Fluorescent Silica Nanoparticles Improve Optical Imaging of Stem Cells Allowing Direct Discrimination between Live and Early-Stage Apoptotic Cells, Small. 8 (2012) 3192–3200. doi:10.1002/smll.201200882.

[14] C. Liu, H. Yu, Q. Li, C. Zhu, Y. Xia, Brighter, More Stable, and Less Toxic: A Host − Guest Interaction- Aided Strategy for Fabricating Fluorescent Silica Nanoparticles and Applying Them in Bioimaging and Biosensing at the Cellular Level, ACS Appl. Mater. Interfaces. 10 (2018) 16291–16298. doi:10.1021/acsami.8b03034.

[15] D.R. Larson, H. Ow, H.D. Vishwasrao, A.A. Heikal, U. Wiesner, W.W. Webb, U. V Park, V. Pennsyl, Silica Nanoparticle Architecture Determines Radiative Properties of Encapsulated Fluorophores, Chem. Mater. 20 (2008) 2677–2684.

[16] F.J. Arriagada, Synthesis of Nanosize Silica in a Nonionic Water-in-Oil Microemulsion : Effects of the Water / Surfactant Molar Ratio and Ammonia Concentration, J Colloid Interface Sci. 211 (1999) 210–220.

[17] I. Miletto, A. Gilardino, P. Zamburlin, S. Dalmazzo, D. Lovisolo, G. Caputo, G. Viscardi, G. Martra, Highly bright and photostable cyanine dye-doped silica nanoparticles for optical imaging: Photophysical characterization and cell tests, Dye. Pigment. 84 (2010) 121–127.

doi:10.1016/j.dyepig.2009.07.004.

[18] G. Alberto, I. Miletto, G. Viscardi, G. Caputo, L. Latterini, S. Coluccia, G. Martra, Hybrid Cyanine - Silica Nanoparticles : Homogeneous Photoemission Behavior of Entrapped Fluorophores and Consequent High Brightness Enhancement, J. Phys. Chem. C. 113 (2009) 21048–21053.

[19] A.J. Winstead, G. Nyambura, R. Matthews, D. Toney, S. Oyaghire, Synthesis of quaternary heterocyclic salts, Molecules. 18 (2013) 14306–14319. doi:10.3390/molecules181114306.

[20] G. Alberto, G. Caputo, G. Viscardi, S. Coluccia, G. Martra, Molecular Engineering of Hybrid Dye − Silica Fluorescent Nanoparticles: In fl uence of the Dye Structure on the Distribution of Fluorophores and Consequent Photoemission Brightness, Chem. Mater. 24 (2012) 2792−2801. doi:10.1021/cm301308g.

[21] J.-H. Yum, P. Walter, S. Huber, D. Rentsch, T. Geiger, F. Nüesch, F. De Angelis, M. Grätzel, M.K. Nazeeruddin, Efficient far red sensitization of nanocrystalline TiO2 films by an unsymmetrical squaraine dye., J. Am. Chem. Soc. 129 (2007) 10320–1. doi:10.1021/ja0731470.

[22] J. Park, N. Barbero, J. Yoon, E. Dell'Orto, S. Galliano, R. Borrelli, J.-H. Yum, D. Di Censo, M. Grätzel, M.K. Nazeeruddin, C. Barolo, G. Viscardi, Panchromatic symmetrical squaraines: a step forward in the molecular engineering of low cost blue-greenish sensitizers for dye-sensitized solar cells, Phys. Chem. Chem. Phys. 16 (2014) 24173–24177. doi:10.1039/C4CP04345F.

[23] R. Borrelli, S. Ellena, C. Barolo, Theoretical and experimental determination of the absorption and emission spectra of a prototypical indolenine-based squaraine dye., Phys. Chem. Chem. Phys. 16 (2014) 2390–8. doi:10.1039/c3cp54298j.

[24] J. Park, C. Barolo, F. Sauvage, N. Barbero, C. Benzi, P. Quagliotto, S. Coluccia, D. Di Censo, M. Grätzel, M.K. Nazeeruddin, G. Viscardi, Symmetric vs. asymmetric squaraines as photosensitisers in mesoscopic injection solar cells: a structure–property relationship study,

Chem. Commun. 48 (2012) 2782. doi:10.1039/c2cc17187b.

[25] A.L. Tatarets, I.A. Fedyunyayeva, T.S. Dyubko, Y.A. Povrozin, A.O. Doroshenko, E.A. Terpetschnig, L.D. Patsenker, Synthesis of water-soluble , ring-substituted squaraine dyes and their evaluation as fluorescent probes and labels, Anal. Chim. Acta. 570 (2006) 214–223. doi:10.1016/j.aca.2006.04.019.

[26] L.I. Markova, E.A. Terpetschnig, L.D. Patsenker, Comparison of a series of hydrophilic squaraine and cyanine dyes for use as biological labels, Dye. Pigment. 99 (2013) 561–570. doi:10.1016/j.dyepig.2013.06.022.

[27] A.P. Legrand, The surface properties of silicas, John Wiley, New York, 1998.

[28] M. Szekeres, J. Tóth, I. Dékány, Specific Surface Area of Stoeber Silica Determined by, Langmuir. 18 (2002) 2678–2685. doi:10.1021/la011370j.

[29] F. Catalano, G. Alberto, P. Ivanchenko, G. Dovbeshko, G. Martra, Effect of Silica Surface Properties on the Formation of Multilayer or Submonolayer Protein Hard Corona: Albumin Adsorption on Pyrolytic and Colloidal SiO2 Nanoparticles, J. Phys. Chem. C. 119 (2015) 26493−26505. doi:10.1021/acs.jpcc.5b07764.

[30] J.R. Lakowicz, Principles of Fluorescence Spectroscopy, 2006.

[31] V. Kabanov, D.J. Press, R.P.S. Huynh, G.K.H. Shimizu, B. Heyne, Assessment of encapsulated dyes' distribution in silica nanoparticles and their ability to release useful singlet oxygen, Chem. Commun. 54 (2018) 6320–6323. doi:10.1039/c8cc03413c.